Published for SISSA by Springer

Received: July 13, 2023
Accepted: September 19, 2023
Published: September 27, 2023

(N)NLO+NLL' accurate predictions for plain and groomed 1-jettiness in neutral current DIS

Max Knobbe,[a] **Daniel Reichelt**[b] **and Steffen Schumann**[a]

[a] *Institut für Theoretische Physik, Georg-August-Universität Göttingen, Friedrich-Hund-Platz 1, 37077 Göttingen, Germany*

[b] *Institute for Particle Physics Phenomenology, Department of Physics, Durham University, Durham DH1 3LE, U.K.*

E-mail: max.knobbe@uni-goettingen.de, daniel.reichelt@durham.ac.uk, steffen.schumann@phys.uni-goettingen.de

Abstract: The possibility to reanalyse data taken by the HERA experiments offers the chance to study modern QCD jet and event-shape observables in deep-inelastic scattering. To address this, we compute resummed and matched predictions for the 1-jettiness distribution in neutral current DIS with and without grooming the hadronic final state using the soft-drop technique. Our theoretical predictions also account for non-perturbative corrections from hadronisation through parton-to-hadron level transfer matrices extracted from dedicated Monte Carlo simulations with Sherpa. To estimate parameter uncertainties in particular for the beam-fragmentation modelling we derive a family of replica tunes to data from the HERA experiments. While NNLO QCD normalisation corrections to the NLO+NLL' prediction are numerically small, hadronisation corrections turn out to be quite sizeable. However, soft-drop grooming significantly reduces the impact of non-perturbative contributions. We supplement our study with hadron-level predictions from Sherpa based on the matching of NLO QCD matrix elements with the parton shower. Good agreement between the predictions from the two calculational methods is observed.

Keywords: Deep Inelastic Scattering or Small-x Physics, Resummation, Higher-Order Perturbative Calculations, Jets and Jet Substructure

ArXiv ePrint: 2306.17736

https://doi.org/10.1007/JHEP09(2023)194

JHEP09(2023)194

Contents

JHEP09(2023)194

1 Introduction

Event shape observables offer great potential for detailed studies of the intriguing dynamics of Quantum Chromodynamics (QCD), thereby providing insight into various strong interaction phenomena. For example, they offer sensitivity to the strong coupling constant α_S, the colour charges of the QCD quanta, and parton density functions, when considering hadronic initial state particles. Predictions for event shape distributions can be obtained from fixed-order perturbation theory, all-orders resummation of logarithmically enhanced contributions, as well as detailed particle-level simulations as provided by Monte Carlo event generators. Accordingly, they form a rather unique testbed for a variety of theoretical approaches, ranging from cutting-edge multi-loop calculations to detailed aspects in the modelling of the non-perturbative parton-to-hadron transition.

Event shapes have played a central role in the QCD measurement program of past e^+e^- collider experiments, see for instance [1–5]. Also at hadron-hadron machines they are considered in studies of hadronic final states. Possibly even more prominently, closely related jet-substructure observables have attracted enormous attention and sparked the development of modern grooming and tagging techniques, see ref. [6] for a recent review. Also in deep-inelastic lepton-nucleon scattering experiments several event shape variables have been measured [7–12]. However, the LEP and HERA experiments phased out in the

years 2000 and 2007, respectively, such that later breakthroughs in calculational methods and modern observable definitions have not yet been fully exploited.

Their complementarity and partially reduced complexity when compared to present day LHC measurements, make the LEP and HERA data a real treasure for additional tests of our theoretical understanding and simulation capabilities. In the past years a small number of re-analyses of the LEP data have been published, see for instance [13–16]. Furthermore, there are efforts to provide open data sets that can directly be used by the entire community [17, 18].

To open the treasure chest of their large data set for modern QCD studies the HERA H1 collaboration has recently started to publish a series of new, fascinating measurements that allow one to confront contemporary state-of-the-art predictions with precise DIS data. Besides their relevance for benchmarking our present day tools, such analyses build an important stepping stone towards future electron-hadron colliders like the EIC at BNL [19, 20] or the LHeC at CERN [21, 22].

We here compile predictions for the 1-jettiness event shape in the Breit frame [23], that is equivalent to the well known thrust variable [24], for the HERA kinematics, i.e. lepton-proton collisions at $\sqrt{s} = 319$ GeV. Furthermore, we consider grooming of the hadronic final states based on the soft-drop method prior to the observable evaluation. We derive differential distributions for groomed and ungroomed τ_1^b differential in the photon virtuality $Q^2 \in [150, 20000]$ GeV^2, and the events inelasticity $y \in [0.05, 0.94]$. We perform Monte Carlo simulations with the Sherpa generator based on next-to-leading-order (NLO) matrix elements for the one- and two-jet final states matched to the parton shower and hadronised using Sherpa's new cluster fragmentation model [25]. To estimate the hadronisation modelling uncertainties in particular related to the beam remnant fragmentation we derive a set of replica tunes [26] to a selection of DIS measurements from the H1 and ZEUS experiments.

Furthermore, we compute resummed predictions at next-to-leading-logarithmic (NLL) accuracy in the observable value based on the implementation of the Caesar resummation formalism [27] in the Sherpa framework [28]. These get matched to the NNLO QCD result for the inclusive DIS process and the NLO matrix elements for the two-jet channel. For the NNLO QCD corrections we rely on an implementation in Sherpa presented in [29]. This results in predictions of NLO + NLL$'$ accuracy for the actual event-shape distributions, while we achieve NNLO precision for the total event rate. In consequence, we refer to our predictions as being (N)NLO+NLL$'$ accurate. To account for non-perturbative corrections we derive parton-to-hadron level transfer matrices differential in the event shape variables that we extract from particle level simulations with Sherpa [30], thereby also accounting for the cluster-model parameter uncertainties through the set of replica tunes to HERA data.

Our calculations are targeted on an upcoming measurement by the H1 experiment, for that preliminary results have recently been presented [31, 32]. Results based on simulations with Sherpa in a similar fiducial phase space have been compared to data from jet-substructure observables in neutral current DIS in [33]. Our study extends earlier work on the simulation of DIS events with Sherpa [34]. Furthermore, this is the first time we include NNLO QCD correction in resummation calculations with Sherpa.

JHEP09(2023)194

The article is organised as follows: in section 2 we introduce the considered observables and define the fiducial phase space used in our study of the hadronic final states produced in ep collisions at HERA. In section 3 we describe the setup used to simulate DIS events with SHERPA as well as the tuning of its beam-fragmentation parameters. In section 4 we present our framework to compile (N)NLO + NLL′ predictions, based on the implementation of the CAESAR formalism in SHERPA. Here, we also present our approach to treat non-perturbative corrections based on transfer matrices extracted from MC simulations, see section 4.1. We present our final (N)NLO + NLL′ + NP results in section 5, alongside with MC predictions from SHERPA. We compile our conclusions and give an outlook in section 6.

2 Phase space and observable definition

We consider deep-inelastic scattering (DIS) of leptons with momentum p of off protons with momentum P at HERA energies, i.e. $E_l = 27.6$ GeV and $E_p = 920$ GeV, resulting in a centre-of-mass energy of $\sqrt{s} = 319$ GeV. Denoting the outgoing lepton momentum as p', we define the momentum difference, at LO carried by the virtual photon, as

$$q = p - p' \equiv (0, 0, 0, -Q)\,, \tag{2.1}$$

where the last equivalence defines the Breit frame, which we will assume whenever frame-specific formulae are given. We also introduce the usual Bjorken variable x_B and inelasticity y

$$x_B = \frac{Q^2}{2P \cdot q}\,, \tag{2.2}$$

$$y = \frac{P \cdot q}{P \cdot p}\,. \tag{2.3}$$

We consider events with $150 < Q^2/\text{GeV}^2 < 2 \cdot 10^4$ and $0.05 < y < 0.94$. No other cuts are applied, but we have studied 1-jettiness in smaller bins of Q^2 and y, and will only discuss a selection of results here.[1]

We take into account all final state particles apart from the outgoing lepton for the calculation of event-shape variables. We study a well known observable, referred to as thrust τ_Q [24] or alternatively 1-jettiness τ_1^b [23]. Several equivalent definitions exist in the literature. For concreteness we define it by dividing the event into a current hemisphere $\mathcal{H}_C$ and a beam hemisphere $\mathcal{H}_B$. Working in the Breit frame, we can introduce two reference vectors

$$n_\pm = (1, 0, 0, \pm 1) \tag{2.4}$$

and denote the hemispheres according to the final state particles momentum fractions along those,

$$\mathcal{H}_C = \{p_i : p_i \cdot n_+ > p_i \cdot n_-\} \quad \text{and} \quad \mathcal{H}_B = \{p_i : p_i \cdot n_+ < p_i \cdot n_-\}\,. \tag{2.5}$$

[1] Results over the full range of Q^2, y in several bins of both variables are available upon request.

JHEP09(2023)194

We can now define thrust as the sum of the longitudinal momentum components of all particles in the current hemisphere. As we prefer to work with an observable that vanishes in the soft limit, i.e. the limit where all final state partons apart from the struck quark have arbitrarily small momenta, we ultimately use

$$\tau = 1 - \frac{2}{Q} \sum_{p_i \in \mathcal{H}_C} p_i^z \,. \tag{2.6}$$

Despite this definition only summing over one of the hemispheres, thrust, i.e. 1-jettiness, is actually sensitive to emissions anywhere in the event, and indeed is a global event shape in the sense of e.g. [27]. Note this statement depends on the precise definition, including the normalisation factor here given by $Q/2$, that differs in the thrust variant we use for tuning in the following.

In addition we study 1-jettiness calculated based on events that have been groomed of soft wide-angle radiation. Soft-drop grooming was first introduced in [35] as a jet substructure technique, including as a special case the modified Mass Drop Tagger [36, 37]. It has since been generalised and applied also to jets at lepton colliders [18, 38] and event shapes at both lepton [38, 39] and hadron [40] colliders. A version applicable to DIS was proposed in [41], based on the CENTAURO jet algorithm [42], that accounts for the forward-backward asymmetry when considering the Breit frame. This sequential cluster algorithm is based on the distance measure between particles with momenta p_i, p_j

$$d_{ij} = (\Delta \bar{z}_{ij})^2 + 2\bar{z}_i \bar{z}_j (1 - \cos \Delta\phi_{ij}) \,, \tag{2.7}$$

$$\text{with} \quad \bar{z}_i = 2\sqrt{1 + \frac{q \cdot p_i}{x_B P \cdot p_i}} \quad \text{and} \quad \Delta \bar{z}_{ij} = \bar{z}_i - \bar{z}_j \,. \tag{2.8}$$

Note that [42] discusses more general functional forms of the distance measure, while we concentrate here on the definition given in [41]. As in all other soft-drop grooming methods the objects of interest, in this case the full event, are first clustered according to this sequential algorithm, and then the reverse clustering history is considered. The last cluster step is undone, and the softness of the softer of the two branches is evaluated. For the DIS case, [41] suggests to use

$$z_i = \frac{P \cdot p_i}{P \cdot q} \tag{2.9}$$

as a measure for softness. The formal soft-drop criterion then reads

$$\frac{\min[z_i, z_j]}{z_i + z_j} > z_{\text{cut}} \,, \tag{2.10}$$

with z_{cut} the grooming parameter. If this is satisfied, i.e. both branches are classified as hard, the algorithm terminates. Otherwise the softer branch (with smaller z) is dropped, and the procedure is repeated with the harder branch. This iteration stops when either eq. (2.10) is satisfied, or there is only one particle left in the hard branch such that no further unclustering is possible.

We finally recalculate 1-jettiness, using eq. (2.6) but restricting the sum to particles in the current hemisphere that have not been dropped during grooming, thereby considering variable values for z_{cut}.

JHEP09(2023)194

3 DIS Monte Carlo simulations with SHERPA

We derive hadron-level predictions for the DIS event shapes using a pre-release version of SHERPA-3.0 [43], that will supersede the current SHERPA-2.2 series [44]. This major release features extended physics-modelling capabilities, including, for example, the automated evaluation of electroweak (EW) corrections at the one-loop order [45–47] or in the Sudakov approximation [48, 49], a complete reimplementation of the cluster hadronisation model [25], as well as an improved user interface based on YAML [50]. To analyse our simulated event samples we employ the RIVET analysis package [51]. For jet clustering we use the CENTAURO plugin [42] within the FASTJET framework [52].

3.1 MEPS@NLO predictions for DIS

The basics of simulating DIS processes by merging parton-shower evolved higher-multiplicity tree-level matrix elements within the SHERPA framework have been presented in [34]. We here lift this to next-to-leading order (NLO) accurate QCD matrix elements. To this end, we consider the massless single and dijet production channels in neutral current DIS at NLO, and three- and four-jets at leading order (LO), i.e.

$$e^- p \to e^- + 1,2\,j\,@\,\mathrm{NLO} + 3,4\,j\,@\,\mathrm{LO}, \tag{3.1}$$

where we consider u, d, s quarks to be massless and add additional LO processes for the remaining massive quarks. The massless and massive channels get matched to the SHERPA Catani-Seymour dipole shower [53] and merged according to the MEPS@NLO [54] and MEPS@LO [55] truncated shower formalism, respectively. The contributing one-loop amplitudes are obtained from OPENLOOPS [56], that employs the COLLIER library [57] for the evaluation of tensor and scalar integrals. All tree-level matrix elements are provided by COMIX [58], and PDFs are obtained from LHAPDF [59].

To determine the perturbative scales entering the calculation, the final states of the multi-parton final states get clustered to a two-to-two core process [55]. For the reconstructed core the factorisation, renormalisation, and parton shower starting scale are set to

$$\mu_\mathrm{F} = \mu_\mathrm{R} = \mu_\mathrm{Q} := \mu_\mathrm{core}\,. \tag{3.2}$$

For jet-associated DIS three configurations need to be distinguished [34]:

(i) virtual photon exchange, i.e. $ej \to ej$, where $\mu^2_\mathrm{core} = Q^2$,

(ii) interaction of the virtual photon with a QCD parton, i.e. $\gamma^* j \to j_1 j_2$, with $\mu^2_\mathrm{core} = m_{\perp,1} m_{\perp,2}$ defined as the product of the two jet transverse masses $m_{\perp,i} = \sqrt{m_i^2 + p^2_{\perp,i}}$ relative to the beam axis,

(iii) and pure QCD channels, i.e. $jj \to jj$, where $\mu^2_\mathrm{core} = -\frac{1}{\sqrt{2}}\left(s^{-1} + t^{-1} + u^{-1}\right)^{-1}$ is a scaled harmonic mean of the Mandelstam variables s, t, u.

Beyond the core process, the arguments of the strong-coupling factors are determined by the clustering algorithm [55]. The merging-scale parameter, separating the different

JHEP09(2023)194

jet-multiplicity contributions, is dynamically set to

$$Q_{\text{cut}} = \frac{\bar{Q}_{\text{cut}}}{\sqrt{1+\bar{Q}^2_{\text{cut}}/Q^2}}\,, \quad \text{using} \quad \bar{Q}_{\text{cut}} = 5\,\text{GeV}\,. \tag{3.3}$$

As parton density functions we use the NNLO PDF4LHC21_40_pdfas set [60] with $\alpha_S(M_Z^2)$=0.118.

To estimate perturbative uncertainties, we consider 7-point variations of the factorisation (μ_F) and renormalisation (μ_R) scales in the matrix element and the parton shower that get evaluated on-the-fly [61], i.e.

$$\left\{\left(\frac{1}{2}\mu_{\text{R}},\frac{1}{2}\mu_{\text{F}}\right),\left(\frac{1}{2}\mu_{\text{R}},\mu_{\text{F}}\right),\left(\mu_{\text{R}},\frac{1}{2}\mu_{\text{F}}\right),(\mu_{\text{R}},\mu_{\text{F}}),(\mu_{\text{R}},2\mu_{\text{F}}),(2\mu_{\text{R}},\mu_{\text{F}}),(2\mu_{\text{R}},2\mu_{\text{F}})\right\}. \tag{3.4}$$

The resummation scale μ_Q we keep fixed. The final uncertainty estimate is derived by forming an envelope of all variations.

3.2 Tuning the beam fragmentation model against HERA data

Ref. [25] presented a new cluster fragmentation model for SHERPA that will be used in SHERPA-3, superseding the old cluster model described in [62], that was used in the SHERPA-1.X [63] and SHERPA-2.X [44] released. A particular feature of the new implementation is a specific treatment of the fragmentation of hadronic clusters that contain beam remnant particles. To calibrate the corresponding model parameters we performed dedicated tunes using HERA data for hadronic final state observables in neutral current DIS.

Broadly speaking, a cluster hadronisation simulation features two basic components, a cluster-formation and a cluster-decay model [64, 65]. Based on the pre-confinement property of QCD [66], finite mass colour neutral mesonic and baryonic clusters can be formed from the final state of a parton shower evolution of a hard scattering event. These primary clusters are then subject to an iterative fission process that ultimately results in the transition to known hadronic resonances, whose decays can be treated by a dedicated package. Both elements of the hadronisation model introduce sets of parameters that need to be carefully adjusted by comparing model predictions and measurements for suitable observables, a process commonly known as tuning.

In ref. [26] the free model parameters were calibrated against hadronic observables measured in electron-positron annihilation experiments. However, in leptonic collisions the beam fragmentation modelling is not probed and the corresponding parameters remained unconstrained. This affects in particular the parametrisation of the decay of clusters that contain a remnant particle of an incident hadron, e.g. a (anti-)quark and (anti-)diquark from the break-up of the incoming proton in DIS. We consider the two-body decay of a beam cluster with flavours f_1 and $\bar{f}_2$, where a (di)quark-flavour pair $f\bar{f}$ is drawn from the vacuum, resulting in

$$\mathcal{C}[f_1\bar{f}_2] \to \mathcal{C}_1[f_1\bar{f}]\,\mathcal{C}_2[f\bar{f}_2]\,. \tag{3.5}$$

To fix the kinematics of the two-body decay in the rest frame of $\mathcal{C}$, the absolute value of the transverse momentum of the decay products $\mathcal{C}_1$ and $\mathcal{C}_2$ is selected according to a Gaussian

JHEP09(2023)194

distribution $\mathcal{N}(0, k_{T,0}^2/2)$ that is truncated at the parton-shower cut-off $p_{T,\min}$, i.e.

$$\mathcal{P}(k_T) \propto \exp\left(-k_T^2/k_{T,0}^2\right) \Theta(p_{T,\min}^2 - k_T^2)\,. \tag{3.6}$$

The parameter $k_{T,0}$ is thereby considered as independent of the incident cluster type. The direction of the two-component $\vec{k}_T$ is picked uniformly in the transverse plane, with f_1 and $\bar{f}_2$ pointing along the positive and negative z-axis, respectively. This leaves one to fix the longitudinal momentum fractions $z^{(1),(2)}$ with respect to the light-like vectors $n_\pm^\mu = (1, 0, 0, \pm 1)$. For the case of a beam-remnant cluster, still working in its rest frame, these are distributed according to

$$\mathcal{P}(z) \propto z^{\alpha_B}(1-z)^{\beta_B} \cdot \exp\left\{-\gamma_B \frac{1}{z}\left(\frac{k_T^2 + (m_{f_1} + m_{\bar{f}_2})^2}{k_{T,0}^2}\right)\right\}\,. \tag{3.7}$$

Note the similarity to the symmetric Lund string fragmentation function [67].

This results in the four-momenta of the decay products being given by

$$p_{\mathcal{C}_1}^\mu = \frac{m_\mathcal{C}}{2}\left(z^{(1)} n_+^\mu + (1 - z^{(2)}) n_-^\mu\right) + k_T^\mu\,, \tag{3.8}$$

$$p_{\mathcal{C}_2}^\mu = \frac{m_\mathcal{C}}{2}\left((1 - z^{(1)}) n_+^\mu + z^{(2)} n_-^\mu\right) - k_T^\mu\,. \tag{3.9}$$

According to eq. (3.7) the relevant free parameters specifically steering the decays of beam clusters are α_B, β_B, and γ_B. To calibrate those we performed dedicated tunes based on a variety of hadronic observables measured by the HERA experiments H1 and ZEUS. The remaining hadronisation parameters are set according to the LEP data tune described in ref. [26].

We employ the Apprentice tuning tool [68], with reference data for DIS analyses at centre of mass energies of $\sqrt{s} = 300\,\text{GeV}$, *i.e.* lepton energies of 27.5 GeV and proton energies of 820 GeV. The tuning requires an initial set of Monte Carlo runs, that are then used to generate a polynomial, bin-wise approximation of the Monte Carlo response with respect to changes in the hadronisation-model parameters. The predictions for the grid points are generated using the calculational setup described in section 3.1.

The selection of observables considered for the tuning includes classic variables sensitive to hadronisation. In particular, we use event-shape distributions like thrust and jet broadening [9], energy flows and charged particle spectra [69, 70] and multiplicities [71, 72], as well as quark fragmentation functions [73, 74]. Further details on the used analyses and observables are provided in appendix A.

Given we consider model parameters newly introduced that have not been tuned before, we have little prior knowledge about their preferred values and thus need to start out with rather wide parameter ranges. To narrow these down, we make an initial pass to get a rough idea of the relevant regions. The corresponding ranges are outlined in table 1. For a second run we restrict the tuning ranges using the results of the exploration run, resulting in an iterative procedure to further narrow down the considered parameter intervals. The initial run, with largely unconstrained parameter values also serves the purpose of filtering out the most sensitive observables from the considered analyses. Observables or observable

JHEP09(2023)194

parameter	parameter tag	tuning range	central tune	uncertainty variation
α_B	`ALPHA_B`	[-1, 20]	14.2	[13.9, 14.8]
β_B	`BETA_B`	[0.5, 4]	1.59	[1.14, 1.60]
γ_B	`GAMMA_B`	[1, 20]	8.11	[8.06, 9.47]

Table 1. AHADIC++ model parameters considered in the tuning. Quoted are the initial parameter interval, the obtained central-tune value, and uncertainty ranges extracted from 7 replica tunes.

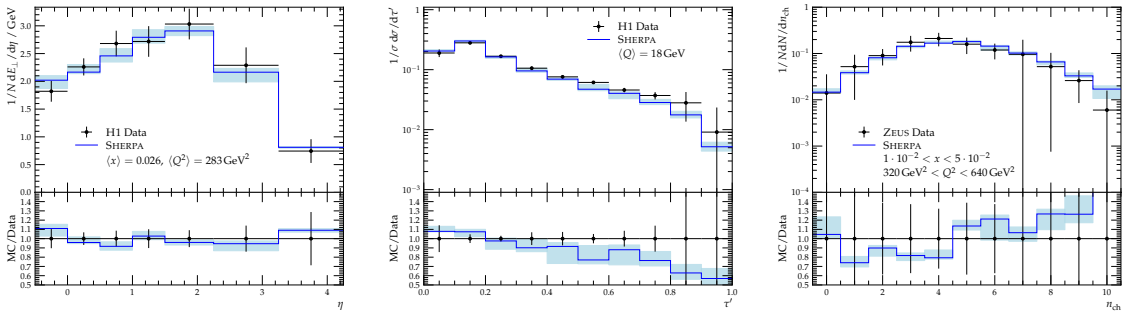

Figure 1. SHERPA predictions for the hadronisation tune, for observables measured by the H1 and ZEUS experiments at $\sqrt{s} = 296\,\text{GeV}$. Shown is the transverse energy flow (left) [69], thrust τ' (center) [9] and the charged particle multiplicity n_{ch} (right) [71]. Note, the statistical uncertainties of the simulated data is small compared to the non-perturbative tuning uncertainties indicated by the blue band.

regions that remain unchanged under the variation of the tuning parameters are not suited for the following tunes and therefore dropped.

Similar to the procedure described in ref. [26], we generate a set of equivalent tunes that only differ by the Monte Carlo runs used to construct the polynomial approximations as described above. The tunes are thus fully equivalent and can be used to estimate the non-perturbative model-parameter uncertainties as illustrated in figure 1 for a selection of data from the HERA experiments. We call these alternative parameter sets replica tunes. To reflect the uncertainty associated with the three beam-fragmentation parameters we here consider seven such replicas, cf. table 1 for the resulting uncertainty variations.

4 (N)NLO + NLL′ resummation for 1-jettiness in DIS

The 1-jettiness observable considered here is equivalent to thrust in DIS, which has originally been resummed at NLL accuracy in [24, 75]. The more general n-jettiness [76, 77] was suggested for lepton-hadron collisions in [78], and has been resummed to NNLL accuracy [79]. For 1-jettiness, analytic fixed order results at LO have been presented in [80], and the NLL calculation has been matched to fixed order at NLO accuracy in [81]. The resummed calculations in this formalism for event shapes in DIS were extended to N^{3}LL in [82]. Grooming for DIS has first been suggested in [41] based on jets defined with the CENTAURO jet algorithm [42]. The same ref. [41] also provided NNLL results for both

JHEP09(2023)194

1-jettiness and jet mass after soft drop grooming. Non-perturbative corrections have there been modelled through a two-parameter shape function [83, 84]. To our knowledge there are no published results studying these observables including matching to fixed order or using a fixed order calculation alone.

4.1 NLL resummation in the CAESAR approach

To perform the NLL resummation of logarithms L of event shapes in DIS we use the implementation of the CAESAR formalism [27] available in the SHERPA framework [28, 85]. For a recursive infrared and collinear (rIRC) safe observable, the cumulative cross section for observable values up to $v = \exp(-L)$ can be expressed to all orders, in general as a sum over partonic channels δ, as follows:

$$\begin{aligned}\Sigma_{\text{res}}(v) &= \sum_{\delta} \Sigma^{\delta}_{\text{res}}(v)\,, \text{ with} \\ \Sigma^{\delta}_{\text{res}}(v) &= \int d\mathcal{B}_{\delta} \frac{d\sigma_{\delta}}{d\mathcal{B}_{\delta}} \exp\left[-\sum_{l\in\delta} R_l^{\mathcal{B}_{\delta}}(L)\right] \mathcal{P}^{\mathcal{B}_{\delta}}(L)\mathcal{S}^{\mathcal{B}_{\delta}}(L)\mathcal{F}^{\mathcal{B}_{\delta}}(L)\mathcal{H}^{\delta}(\mathcal{B}_{\delta})\,,\end{aligned} \tag{4.1}$$

where $\frac{d\sigma_{\delta}}{d\mathcal{B}_{\delta}}$ is the fully differential Born cross section for channel δ and $\mathcal{H}$ implements the kinematic cuts applied to the Born phase space $\mathcal{B}$. For a 2-jet observable like thrust in DIS, there is only one relevant partonic Born channel, corresponding to an incoming and an outgoing quark. This also implies that the soft function $\mathcal{S}$, which implements colour evolution, is trivial in our case. Further, since we are dealing with an additive observable, the multiple emission function $\mathcal{F}$ is simply given by $\mathcal{F}(L) = e^{-\gamma_E R'}/\Gamma(1+R')$, with $R'(L) = \partial R/\partial L$ and $R(L) = \sum_{l\in\delta} R_l(L)$. The collinear radiators R_l for the hard legs l were computed in [27] for a general observable V scaling for the emission of a soft-gluon of relative transverse momentum $k_t^{(l)}$ and relative rapidity $\eta^{(l)}$ with respect to leg l as

$$V(k) = \left(\frac{k_t^{(l)}}{\mu_Q}\right)^a e^{-b_l\eta^{(l)}} d_l\left(\mu_Q\right) g_l\left(\phi\right)\,. \tag{4.2}$$

For the case of 1-jettiness we are focusing on in this publication, we have $a = b_l = 1$, and fixing $\mu_Q^2 = Q^2$ also $d_l g_l = 1$ since there is no dependence on the azimuthal angle ϕ. The precise form of the logarithm can be varied according to

$$L \to \ln\left[\frac{x_L}{v} - x_L + 1\right] \to \ln\frac{x_L}{v} \quad \text{as} \quad v \to 0\,, \tag{4.3}$$

to estimated the impact of sub-leading logarithms, while leaving the distribution at the kinematic endpoint $v \sim 1$ unchanged. Note this implies an additional contribution to $R_l(L)$ to restore NLL accuracy.

The PDF factor $\mathcal{P}$, in our study applicable only to the hadronic beam, is here given by

$$\mathcal{P} = \frac{f_q(x, e^{-2L/(a+b)}\mu_F^2)}{f_q(x,\mu_F^2)}\,, \tag{4.4}$$

corrects for the true initial-state collinear scale. We thereby account for the full DGLAP evolution by calculating a simple ratio. For the purpose of matching to a fixed order

JHEP09(2023)194

calculation, we also need the expansion of the ratio to a given order in α_s. We generally follow the approach of [27] to implement the expansion of a leading order approximation. This of course introduces additional effects beyond our considered logarithmic accuracy. We argue it is safe to ignore those, given the generally small numerical size of these contributions as seen for example in [28]. We here for the first time apply the CAESAR implementation in SHERPA to an observable that is sensitive to the PDF ratio (note this only applies to the ungroomed version of thrust) and at the same time match to the NLO calculation for the differential distribution and the NNLO result for the inclusive DIS process. We hence need to take care of the expansion to one order higher. Following [27], the numerator of eq. (4.4) can to NLL accuracy be written and expanded in powers of α_s as

$$\begin{aligned}\mathbf{f}(x, e^{-2L/(a+b)}\mu_F^2) &= \exp\left[-T\left(\frac{L}{a+b}\right)\mathbf{P}\otimes\right]\mathbf{f}(x,\mu_F^2)\\ &\sim 1 - \left(T^{(1)}\left(\frac{L}{a+b}\right) + T^{(2)}\left(\frac{L}{a+b}\right)\right)\mathbf{P}\otimes\mathbf{f}(x,\mu_F^2)\\ &\quad + \frac{1}{2}\left(T^{(1)}\left(\frac{L}{a+b}\right)\right)^2\mathbf{P}\otimes\mathbf{P}\otimes\mathbf{f}(x,\mu_F^2) + \mathcal{O}\left(\alpha_s^3\right), \end{aligned} \tag{4.5}$$

where $T^{(i)}$ denotes the ith term obtained by expanding the integrated strong coupling

$$T(L) = -\frac{1}{\pi\beta_0}\ln(1-2\alpha_s\beta_0 L) \tag{4.6}$$

in powers of α_s. The bold-faced symbols represent matrices (of splitting functions, $\mathbf{P}$) and vectors ($\mathbf{f} = (f_u, f_d, f_s, \dots)$) in flavour space, and the convolution is given by

$$\mathbf{P}\otimes\mathbf{f}(x,\mu_F^2) = \int_x^1 \frac{dz}{z}\mathbf{P}\left(\frac{x}{z}\right)\mathbf{f}(z,\mu_F^2)\,. \tag{4.7}$$

New terms at $\mathcal{O}(\alpha_s^2)$ hence originate from the higher order expansion of T, mixed terms with other parts of the resummation multiplying the leading order expansion, and the convolution of two splitting functions with the PDF in the last line of eq. (4.5). The last one is the only one that requires a non-trivial implementation. We use the expressions from [86] for convoluted splitting functions, and solve the final integral for the convolution with the PDF through Monte Carlo integration, as done at leading order.

We match our resummed calculation in the multiplicative matching scheme along the lines of [85], which we briefly recap here. The matching to fixed order is done at the level of cumulative distributions $\Sigma(v)$. Note that we have dropped the label for the partonic channel since in our case there is a single one only. We expand the inclusive cross section σ_{fo} as well as the fixed-order and resummed cumulative distributions, Σ_{fo} and Σ_{res} in series of α_s:

$$\sigma_{\text{fo}} = \sigma^{(0)} + \sigma_{\text{fo}}^{(1)} + \sigma_{\text{fo}}^{(2)} + \dots\,, \tag{4.8}$$

$$\Sigma_{\text{fo}}(v) = \sigma^{(0)} + \Sigma_{\text{fo}}^{(1)}(v) + \Sigma_{\text{fo}}^{(2)}(v) + \dots\,, \tag{4.9}$$

$$\Sigma_{\text{res}}(v) = \sigma^{(0)} + \Sigma_{\text{res}}^{(1)}(v) + \Sigma_{\text{res}}^{(2)}(v) + \dots\,, \tag{4.10}$$

where the number in parentheses indicates the respective order in α_s, and $\sigma^{(0)}$ denotes the Born-level cross section. Our final matched expression for the cumulative distribution,

JHEP09(2023)194

with the dependencies on the observable value suppressed, reads:

$$\Sigma_{\text{matched}} = \Sigma_{\text{res}} \left(1 + \frac{\Sigma^{(1)}_{\text{fo}} - \Sigma^{(1)}_{\text{res}}}{\sigma^{(0)}} + \frac{\Sigma^{(2)}_{\text{fo}} - \Sigma^{(2)}_{\text{res}}}{\sigma^{(0)}} - \frac{\Sigma^{(1)}_{\text{res}}}{\sigma^{(0)}} \frac{\Sigma^{(1)}_{\text{fo}} - \Sigma^{(1)}_{\text{res}}}{\sigma^{(0)}} \right) . \tag{4.11}$$

Note that, compared to our earlier works, we use $\Sigma^{(2)}$ directly, thus reproducing the inclusive cross section to one order higher, i.e. NNLO, what requires the calculation of $\sigma^{(2)}_{\text{fo}}$. Importantly, the resummed NLL result Σ_{res} is multiplied by

$$\frac{\Sigma^{(1)}_{\text{fo}} - \Sigma^{(1)}_{\text{res}}}{\sigma^{(0)}} \to \frac{\alpha_s}{2\pi} C_1 \quad \text{as} \quad v \to 0 \,. \tag{4.12}$$

We refer to the distribution that includes all NLL terms in Σ_{res} and additionally the coefficient C_1 as NLL$'$ accurate. Through this matching procedure we achieve a formal accuracy of NLO + NLL$'$ for the differential distribution and NNLO for the inclusive event rate, referred to as (N)NLO + NLL$'$ in what follows.

In addition to the perturbative contribution described above, there is a significant non-perturbative component to the distribution of event shapes, that we necessarily need to take into account in order to accurately describe actual collider data. While it has been shown in various circumstances that soft-drop grooming reduces the impact of hadronisation corrections, see for example [30, 38–40, 83, 87], it is typically still necessary to account for a remaining small non-perturbative contribution. We here adopt the approach of [30] to extract transfer matrices from Monte Carlo simulations. Transfer matrices are defined as

$$\mathcal{T}_{hp} = \frac{\int dP \, \frac{d\sigma}{dP} \Theta_p(P) \, \Theta_h(H(P))}{\int dP \, \frac{d\sigma}{dP} \Theta_p(P)} \,, \tag{4.13}$$

with

$$\Theta_p(P) = \prod_{i=1}^{m} \theta(V_i(P) - v^{\min}_{p,i}) \theta(v^{\max}_{p,i} - V_i(P)) \,, \tag{4.14}$$

$$\Theta_h(H(P)) = \prod_{i=1}^{m} \theta\left(V_i(H(P)) - v^{\min}_{h,i}\right) \theta\left(v^{\max}_{h,i} - V_i(H(P))\right) \,, \tag{4.15}$$

for a transition between the parton level phase space P and the corresponding hadron level configuration $H(P)$, characterised by a set of observables V_i that can be calculated on both of them. For our purpose, we assume that the requirements on the DIS kinematics, cf. section 2, sufficiently fix the remaining degrees of freedom other than 1-jettiness τ. This first of all means that we do not allow non-perturbative corrections to change the underlying Born kinematics, i.e. the Q^2, y bin, in contrast to, for example, measurements performed on jets with a potentially affected transverse momentum spectrum. On the other hand this implicitly assumes that it is valid to average the corrections for all configurations with a common 1-jettiness value. Hence, we are only concerned with events migrating between different bins in τ within a given Q^2, y bin. The transfer matrices as defined above can readily be extracted from the Sherpa event generator by analysing the different stages of the events evolution, i.e. after parton showering but before hadronisation

JHEP09(2023)194

and thereafter. For practical details of our event generation setup see section 3. Our final results are then calculated from the resummed and matched parton level bins $\Delta\sigma_p^{\mathrm{PL}}$ as

$$\Delta\sigma_h^{\mathrm{HL}} = \sum_p \mathcal{T}_{hp}\, \Delta\sigma_p^{\mathrm{PL}} \,. \tag{4.16}$$

4.2 Grooming in DIS

The framework described above has already been employed to obtain resummed predictions for soft-drop thrust in lepton-lepton collisions at NLO + NLL′ precision [39], for soft-drop groomed hadronic event shapes [40] and groomed jet substructure observables at the LHC [30, 87, 88]. The extensions made in [40] to accommodate the phase space constraints implied by soft-drop grooming, with general parameters z_{cut} and β, are directly applicable here. Note that [41] does not define a $\beta \neq 0$ version of grooming in DIS, and we make no attempt here to extend it.

The applicability of the results from [40] to DIS event shapes relies on two statements. First, within the current hemisphere the phase space constraints to radiation in the soft and collinear limits correspond to the case of final state radiation in general hadronic collisions. Second, in the beam hemisphere any soft and collinear radiation is groomed away. Accordingly, we can treat radiation in $\mathcal{H}_B$ equivalent to the initial state radiation case in [40], even if the precise shape of the phase space boundary is different, but such difference does not enter at NLL accuracy. We analyse the behaviour of the CENTAURO algorithm and the associated soft-drop grooming variant in the language of the CAESAR framework in the following to illustrate this. Recall that we are working in the Breit frame. At NLL accuracy, we have to take into account ensembles of soft particles, well separated in rapidity, around a Born configuration consisting of the proton momentum

$$P^\mu = \frac{Q}{2x_B} n_+^\mu \tag{4.17}$$

and the outgoing struck quark in n_- direction. The virtual photon carries momentum

$$q = \frac{Q}{2}(n_- - n_+) \,. \tag{4.18}$$

We parameterise the momenta of additional soft gluons as

$$k_i^\mu = k_t^i \left(\frac{e^{\eta_i}}{2} n_-^\mu + \frac{e^{-\eta_i}}{2} n_+^\mu + n_\perp^\mu \right) , \tag{4.19}$$

where $n_\perp$ is a transverse unit vector perpendicular to n_+ and n_-. The variable introduced in the CENTAURO algorithm, cf. eq. (2.8), can be written using the phase space variables η_i, k_t^i as

$$\bar{z}_i = 2e^{-\eta_i} \,, \tag{4.20}$$

such that the expression for the distance measure, cf. eq. (2.7), becomes

$$d_{ij} = 4\left(e^{-2\eta_i} + e^{-2\eta_j} + 2e^{-(\eta_i+\eta_j)} \cos\Delta\phi_{ij} \right) \sim 4e^{-2\eta_i} \,, \tag{4.21}$$

JHEP09(2023)194

where we have identified the behaviour for strong ordering in η, $\eta_i \ll \eta_j$. In this limit, the algorithm builds up a single jet containing the hard quark by adding the next remaining gluon that is most collinear to this jet. The last clustering will add the gluon most collinear to the beam direction to the jet. If all gluons are separated in rapidity well enough, there are no other clusters to be taken care of.

From this discussion it is clear that all comparisons of scales during soft drop will be between a soft gluon and a jet containing the hard quark. At Born level, the four-momentum of the jet will be approximately that of the quark, and the gluon will be the softer of the two. With this in mind the hardness measure for soft drop for soft momentum k_i can be written as

$$z_i \sim \frac{k_t^i}{Q} e^{\eta_i} \,. \tag{4.22}$$

Within the current hemisphere, the phase space restriction, on an emission that passes the soft-drop criterion, is given by

$$\frac{k_t e^{\eta}}{Q} > z_{\text{cut}} \,, \tag{4.23}$$

which precisely matches the one given in [40] for $\beta = 0$ (see section 3.4 point (iv), and note that the hard quark has energy $Q/2$ in the Breit frame).

Note that particles outside of the current hemisphere will enter in eq. (4.23) with negative rapidity η. They will hence be groomed away unless they are at very high k_t, only causing logarithms of z_{cut}. We note again that the precise shape of the phase space boundary is different from what is given in [40] for initial states. The main point is however that only logarithms of z_{cut} are produced, which we ignore noting again that we work in the limit $v \ll z_{\text{cut}}$.

4.3 Calculational tools and setup

As already stated, the resummation calculation for 1-jettiness is accomplished with the CAESAR plugin to SHERPA that hooks into the event generation framework.[2] SHERPA thereby provides all the process management, and gives access to the COMIX matrix element generator [58], as well as phase-space integration and event-analysis functionalities. We make use of SHERPA's interface to LHAPDF [59] and use the PDF4LHC_40_pdfas PDF set, as we do for the parton-shower simulations outlined in the previous section. The value of the strong coupling is set accordingly, i.e. $\alpha_S(M_Z^2) = 0.118$. The SHERPA framework is also used to compile all the required higher-order tree-level and one-loop calculations. For the NLO QCD computations we use the SHERPA implementation of the Catani-Seymour dipole subtraction [89] and the interfaces to the RECOLA [90, 91] and OPENLOOPS [92] one-loop amplitude generators. The calculation of NNLO accurate predictions for DIS has been automated in SHERPA in [29], and we use it to compute cross sections $\sigma_{\text{fo}}^{(2)}$ at order α_s^2 differential in Q^2 and y to achieve overall NNLO accuracy for inclusive cross sections. This corresponds to an accuracy of the distribution differential in thrust at NLO, and we refer to the combined accuracy of our fixed order predictions including cross sections as (N)NLO.

[2] Note, during the course of this work the plugin has been ported to the SHERPA-3.0 release series.

JHEP09(2023)194

The plugin implements the building blocks of the CAESAR master formula eq. (4.1), along with the necessary expansion in α_s used in the matching with fixed-order calculations. The building blocks are evaluated fully differentially for each Born-level configuration $\mathcal{B}_\delta$ of a given momentum configuration. Jet clustering and grooming functionalities are accessed through the interface of SHERPA to FASTJET [52]. Non-perturbative corrections are extracted from dedicated runs of the SHERPA generator using the identical setup described in section 3, thereby employing the functionality of the RIVET analysis tool to provide access to intermediate evolution stages through the HEPMC event record [93].

5 Results for (groomed) 1-jettiness in DIS

Having outlined our calculational techniques for describing hadronic final state observables in neutral current DIS, we can finally present our numerical results for the 1-jettiness event shape. We begin by discussing selected results for the ungroomed case. We have compiled predictions for a wide range of Q^2 values, i.e. $Q^2 \in [150, 20000]$ GeV^2. Furthermore, we consider the production cross section differential in the events inelasticity, thereby covering the region $y \in [0.05, 0.94]$. For brevity, we here focus on three kinematic regions corresponding to medium values of $y \in [0.4, 0.7]$ and rather low ($Q^2 \in [150, 200]\,\text{GeV}^2$), medium ($Q^2 \in [440, 700]\,\text{GeV}^2$) and high ($Q^2 \in [3500, 8000]\,\text{GeV}^2$) photon virtuality.

Along with the central predictions we show error bands indicating the perturbative uncertainty obtained from 7-point variations of μ_R, μ_F, in both the shower and the semi-analytic calculation, and in addition a variation of $x_L = 0.5, 2$ in the latter, cf. eq. (4.3). Furthermore, we include an uncertainty estimate related to the tuning of beam-fragmentation parameters based on replica tunes, see section 3.2. Generally, this contribution is found to be rather small compared to the perturbative uncertainties. We observe the overall uncertainties for the NLO QCD matrix element plus parton-shower simulations and the resummation predictions to be of similar sizes.

We first analyse the behaviour of the NLO + NLL$'$ resummation calculation upon inclusion of the NNLO normalisation correction and non-perturbative effects. To this end we compile in figure 2 corresponding predictions for the three kinematic regions specified before. From the lower panels, showing the ratio to the respective NLO + NLL$'$ result, it can be read off, that correcting the normalisation to NNLO accuracy has a rather small impact. The differential cross section receives a small negative correction, of at most a few percent at small τ in the lower Q^2 region. Note, however, that even the smallest Q^2 values in this analysis remain sizeable compared to the overall range accessible for the HERA experiments. Somewhat more significant is the reduction in the perturbative uncertainties when going from NLO to NNLO, in particular for the bulk of the distributions, i.e. low values of 1-jettiness.

Next, we consider the inclusion of non-perturbative corrections based on the transfer-matrix approach described in section 4.1. As clearly visible in figure 2 these significantly alter the shape of the distributions, introducing a sizeable shift towards larger 1-jettiness values. In particular for the low and medium Q^2 region the first bin gets almost entirely depopulated. In contrast, for values of $\tau \approx 0.1 \ldots 0.2$ corrections can reach up to +100%.

JHEP09(2023)194

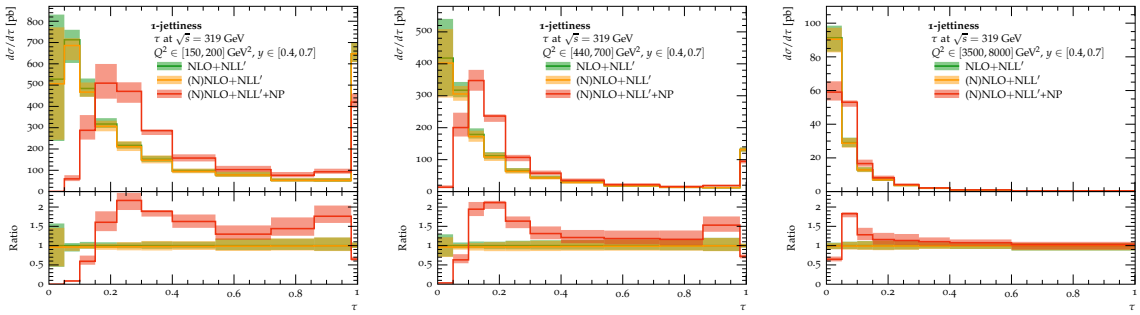

Figure 2. Distributions of ungroomed 1-jettiness in selected $y - Q^2$ bins, at different stages of the calculation, at NLO + NLL′ accuracy, including the normalisation at NNLO ((N)NLO + NLL′) accuracy, and including non-perturbative corrections. All results correspond to DIS kinematics with $y \in [0.4, 0.7]$ and the plots represent from left to right regions of $Q^2/\text{GeV}^2 \in [150, 200]$, $[440, 700]$, and $[3500, 8000]$, respectively. The lower panels present the ratio to the plain NLO + NLL′ result.

The effect of hadronisation corrections is less pronounced at higher Q^2. We furthermore note, that the non-perturbative corrections through the bin migration via transfer matrices partially compensate the dependence of the perturbative calculation on scale variations and in particular of μ_R.

We close this first discussion of the resummed predictions for ungroomed 1-jettiness by pointing to the distinct peak at $\tau \approx 1$ for the low and medium Q^2 distributions, emerging after a significant decline of the differential cross section from lower to larger observable values. For the given observable definition the configuration $\tau = 1$ can be attributed to events with an empty current hemisphere $\mathcal{H}_C$ [80]. Such configurations first appear when considering the NLO real-emission correction to the DIS process, when both final state partons feature negative longitudinal momenta in the Breit frame, such that 1-jettiness defaults to 1, see eq. (2.6). We here account for these configurations through matching to the exact NLO QCD result for τ, i.e. including the full $\mathcal{O}(\alpha_S)$ corrections to the two-parton channel. It can be observed, that hadronisation corrections reduce the amount of $\tau \approx 1$ events, what can be expected, as the fragmentation of partons originally in the beam hemisphere might spill over hadrons in the current hemisphere.

We now turn to the presentation of the hadron level results from MEPS@NLO simulations with Sherpa as outlined in section 3 and compare those to the (N)NLO + NLL′ + NP predictions. In figure 3 we compare the respective results for the three considered kinematic regions. We observe an overall fair agreement between the matrix element improved shower simulations at hadron level obtained from Sherpa and the resummed and matched calculation at (N)NLO + NLL′ + NP accuracy, corrected for non-perturbative effects. In general the merged prediction features a somewhat harder spectrum, i.e. favours somewhat larger observable values. This might also be attributed to the inclusion of the exact tree-level three- and four-jet matrix elements, see eq. (3.1). These contributions feature LO scale dependence and are thus the source for the somewhat enlarged theoretical uncertainties in the shower simulation towards larger values of τ. However, the regions of small 1-jettiness agree within uncertainties for all three kinematic regions, up until the peak of the respec-

JHEP09(2023)194

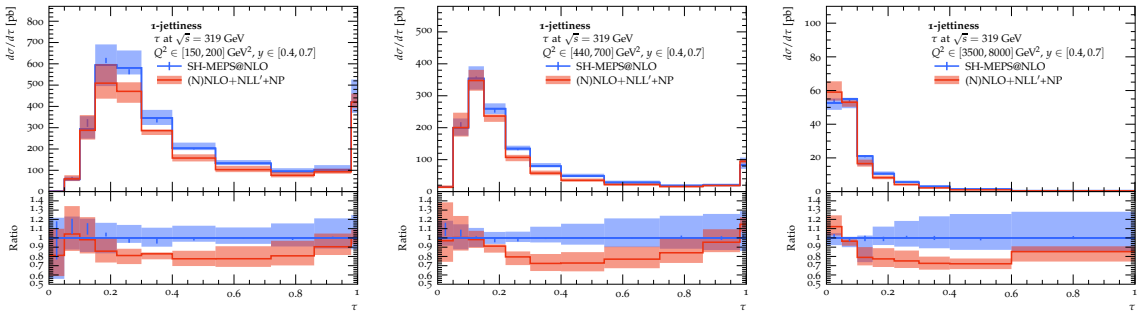

Figure 3. Distributions of 1-jettiness in selected $y - Q^2$ bins, i.e. $y \in [0.4, 0.7]$ and, from left to right, $Q^2/\text{GeV}^2 \in [150, 200]$, $[440, 700]$, and $[3500, 8000]$, respectively. Shown are hadron level MEPS@NLO predictions from SHERPA and results at (N)NLO + NLL′ + NP accuracy. The lower panels present the ratio to the MEPS@NLO result.

tive distribution. Towards the kinematic endpoint, the two approaches tend to agree again, with both calculations predicting very similar cross sections for events with $\tau \sim 1$.

Besides the plain 1-jettiness event shape we here also consider the effect of soft-drop grooming the hadronic final state. In figure 4 we show resummed predictions for groomed 1-jettiness, referred to as τ^{SD} in what follows, integrated over the full Q^2 range, i.e. $Q^2 \in [150, 20000]$ GeV^2, and the inelasticity region $y \in [0.2, 0.7]$. We compiled predictions for three commonly considered values of z_{cut}, namely $z_{\text{cut}} = 0.05, 0.1, 0.2$, thereby always assuming the angular grooming parameter $\beta = 0$. As seen for the ungroomed case, we note rather small effects of the NNLO normalisation corrections compared to the NLO + NLL′ calculation. Also the systematic uncertainties hardly change from NLO to NNLO. However, the size of the non-perturbative corrections is significantly reduced relative to the ungroomed case, staying below 50% and being largely flat over a wide range of τ^{SD}, apart from very low values of 1-jettiness and at the endpoint $\tau^{\text{SD}} \sim 1$. This confirms the potential of soft-drop grooming to mitigate hadronisation effects for event shape observables also in DIS, seen before in e^+e^- [38, 39] and pp collisions [40].

The comparison of the (N)NLO + NLL′ + NP results with hadron level simulations at MEPS@NLO accuracy is presented in figure 5. For all the z_{cut} values, we observe good agreement between our SHERPA simulation and the resummation calculation somewhat better than for the ungroomed case. In all three cases, the (N)NLO + NLL′ + NP calculation predicts a larger cross section in the $\tau \sim 1$ bin, although still compatible within the uncertainty of the event generator for $z_{\text{cut}} = 0.05$ and the combined uncertainty for both calculations for $z_{\text{cut}} = 0.1$. Apart from this last bin, for these two z_{cut} values the resummation calculation is consistently below the SHERPA simulation. In the case of $z_{\text{cut}} = 0.05$, this happens flat over the full spectrum $\tau^{\text{SD}} < 1$, while for increasing z_{cut} a slight shape develops, with the (N)NLO + NLL′ + NP cross section decreasing faster for $\tau^{\text{SD}} < z_{\text{cut}}$ than what is seen in the Monte Carlo simulation.

It will be interesting to compare the (N)NLO + NLL′ + NP predictions and the SHERPA MEPS@NLO simulations with the data of upcoming measurements by the H1 experiment. This will shed light on the found deviations between the two sets of predictions and possibly

JHEP09(2023)194

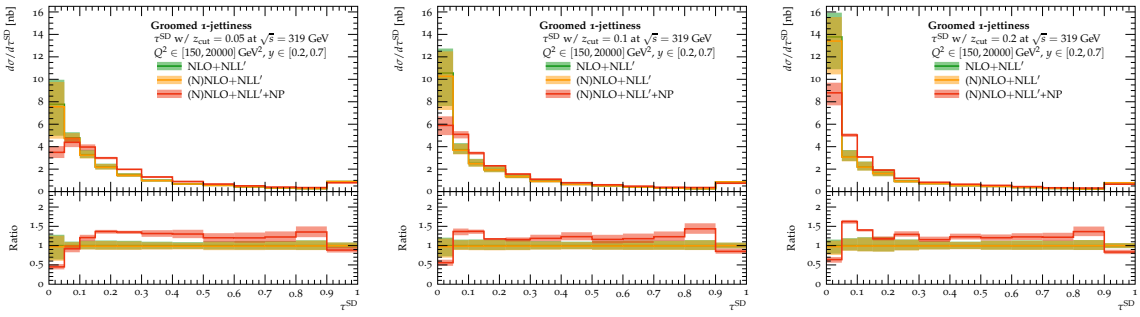

Figure 4. Distributions of groomed 1-jettiness, at different stages of the calculation, at NLO + NLL′ accuracy, including the normalisation at NNLO ((N)NLO + NLL′) accuracy, and including non-perturbative corrections. From left to right the plots represent predictions for the grooming parameter $z_{\text{cut}} = 0.05, 0.1, 0.2$, respectively. The lower panels present the ratio to the plain NLO + NLL′ result.

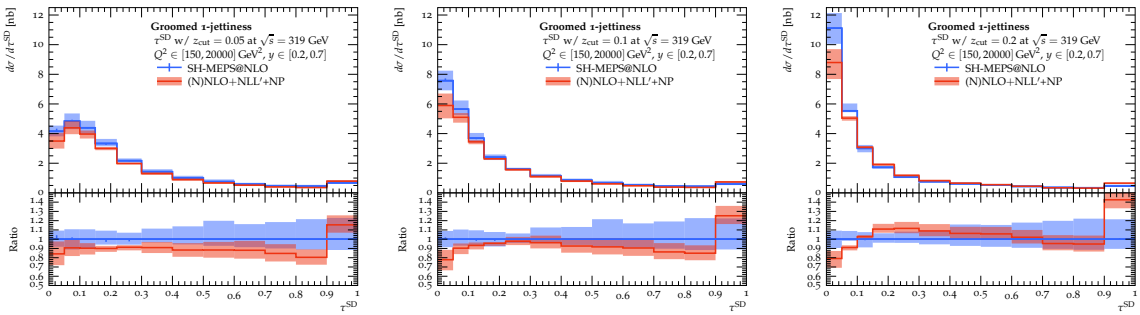

Figure 5. Distributions of groomed 1-jettiness. Shown are hadron level MEPS@NLO predictions from SHERPA and results at (N)NLO + NLL′ + NP accuracy. From left to right the plots represent predictions for the grooming parameter $z_{\text{cut}} = 0.05, 0.1, 0.2$, respectively. The lower panels present the ratio to the MEPS@NLO result.

guide the development of yet improved theoretical predictions, e.g. through the inclusion of next-to-next-to-leading logarithmic corrections.

6 Conclusions

We presented the calculation of theoretical predictions for the 1-jettiness event shape in neutral current DIS at HERA energies. The here considered 1-jettiness observable, evaluated in the Breit frame, is equivalent to the well-known thrust variable that has been widely studied at lepton and hadron colliders. Besides plain 1-jettiness we also considered its variant after soft-drop grooming the hadronic final state using different values of the grooming parameter z_{cut}. We consider the triple-differential cross section in the observable, momentum transfer Q^2, and the events inelasticity y.

Based on the CAESAR formalism we derive NLL accurate results matched to the exact NLO QCD matrix element for the two-jet DIS matrix element. Furthermore, we include the exact NNLO QCD corrections to the inclusive DIS process, thereby achieving full

JHEP09(2023)194

NNLO accuracy for the integrated observable distribution. We furthermore correct our results of (N)NLO + NLL′ accuracy for non-perturbative hadronisation effects through a transfer matrix that takes into account migration in the observable value when going from parton to hadron level. The corresponding corrections have been extracted from Monte Carlo simulations at MEPS@NLO accuracy with the SHERPA generator. To this end, we have performed tunes of the beam-fragmentation parameters of SHERPA's new cluster fragmentation model against data from the H1 and ZEUS experiments. We thereby also derived replica tunes that account for the parametric uncertainties.

For plain 1-jettiness we have shown results for three kinematic regions, corresponding to medium inelasticity y and ranges of rather low, medium, and high Q^2 values. While the impact of the NNLO contributions is found to be very small, hadronisation corrections significantly sculpt the differential distributions, pushing events from lower to larger 1-jettiness values. When comparing the hadronisation corrected (N)NLO + NLL′ predictions with hadron level predictions from SHERPA good agreement is found, with larger deviations dominantly in the region $0.2 < \tau < 0.6$. Quite good agreement is found regarding events at the endpoint of the distribution, i.e. $\tau \simeq 1$. For the low and medium Q^2 regions the distribution here develops a significant peak, that can be attributed to events with an empty current hemisphere.

For the soft-drop groomed variant of 1-jettiness we have shown predictions for three values of z_{cut}, integrated over a wide range of Q^2, i.e. $Q^2 \in [150, 20000]$ GeV^2, and $y \in [0.2, 0.7]$. For all values of z_{cut} non-perturbative corrections to the resummed predictions get significantly reduced, when comparing to the ungroomed case. Furthermore, an improved agreement with the hadron level predictions from SHERPA is found.

It will be exciting to confront the two types of predictions with actual data from the HERA collider that are currently being analysed by the H1 experiment. We can expect that in particular for the ungroomed 1-jettiness observable data should be able to discriminate between the two predictions. This will motivate and guide the development and advancement of the theoretical predictions. For DIS parton shower simulations there are recent developments towards the inclusion of NNLO QCD corrections [29] and to achieve formal NLL accuracy [94–97]. This would allow to match the precision of the analytic predictions we presented in this study. Improving the analytic calculation might require the inclusion of higher-logarithmic corrections or improved means to account for non-perturbative corrections. Furthermore, a detailed analysis of systematic differences between analytic NLL resummation and shower algorithms implementing unitarity and momentum conservation along the lines of [98] might help to pin down the origin of the observed differences.

Acknowledgments

We would like to thank Daniel Britzger and Henry Klest for triggering us to dive into DIS event shapes and a very fruitful communication. We furthermore thank Johannes Hessler and Vinicius Mikuni for discussions. We are indebted to Stefan Höche for assistance with the NNLO corrections and we are grateful to Frank Krauss for help with SHERPA's new beam fragmentation model.

JHEP09(2023)194

RIVET Analysis name [reference]	Observables	Virtuality range [GeV^2]
H1_2006_I699835 [9]	thrust, jet broadening	$Q^2 \in [256, 400]$
H1_1994_S2919893 [70]	transverse energy flow	$Q^2 \in [10, 100]$
	energy-energy correlation	$Q^2 \in [10, 100]$
H1_1995_I394793 [73]	quark fragmentation functions	$Q^2 > 100$
H1_1996_I422230 [72]	charged multiplicity distributions	$Q^2 \in [10, 1000]$
H1_1996_I424463 [99]	charged particle spectra	$Q^2 \in [5, 50]$
H1_1997_I445116 [74]	quark fragmentation functions	$Q^2 \in [100, 8000]$
	charged hadron energy spectra	$Q^2 \in [100, 8000]$
H1_2000_S4129130 [69]	transverse energy flow	$Q^2 \in [10, 2200]$

Table 2. RIVET analysis tags, observables and corresponding photon virtuality ranges used for the tuning.

MK and SS acknowledge support from BMBF (05H21MGCAB) and funding by the Deutsche Forschungsgemeinschaft (DFG, German Research Foundation) — project number 456104544 and 510810461. DR is supported by the STFC IPPP grant (ST/T001011/1).

A Tuning details

We here collate more detailed information on the tuning of the AHADIC++ beam-fragmentation parameters. The RIVET analyses and considered observable measurements by the H1 and ZEUS HERA experiments used for the tuning are summarised in table 2.

References

[1] ALEPH collaboration, *Measurement of the strong coupling constant α_s from global event shape variables of hadronic Z decays*, *Phys. Lett. B* **255** (1991) 623 [INSPIRE].

[2] OPAL collaboration, *A measurement of global event shape distributions in the hadronic decays of the Z^0*, *Z. Phys. C* **47** (1990) 505 [INSPIRE].

[3] L3 collaboration, *Determination of α_s from hadronic event shapes measured on the Z^0 resonance*, *Phys. Lett. B* **284** (1992) 471 [INSPIRE].

[4] DELPHI collaboration, *Energy dependence of event shapes and of α_s at LEP-2*, *Phys. Lett. B* **456** (1999) 322 [INSPIRE].

[5] DELPHI collaboration, *A study of the energy evolution of event shape distributions and their means with the DELPHI detector at LEP*, *Eur. Phys. J. C* **29** (2003) 285 [hep-ex/0307048].

[6] S. Marzani, G. Soyez and M. Spannowsky, *Looking inside jets: an introduction to jet substructure and boosted-object phenomenology*, Springer (2019) [DOI:10.1007/978-3-030-15709-8] [INSPIRE].

JHEP09(2023)194

[7] H1 collaboration, *Measurement of event shape variables in deep inelastic ep scattering*, *Phys. Lett. B* **406** (1997) 256 [hep-ex/9706002] [INSPIRE].

[8] H1 collaboration, *Investigation of power corrections to event shape variables measured in deep inelastic scattering*, *Eur. Phys. J. C* **14** (2000) 255 [*Erratum ibid.* **18** (2000) 417] [hep-ex/9912052] [INSPIRE].

[9] H1 collaboration, *Measurement of event shape variables in deep-inelastic scattering at HERA*, *Eur. Phys. J. C* **46** (2006) 343 [hep-ex/0512014].

[10] ZEUS collaboration, *Event shape analysis of deep inelastic scattering events with a large rapidity gap at HERA*, *Phys. Lett. B* **421** (1998) 368 [hep-ex/9710027] [INSPIRE].

[11] ZEUS collaboration, *Measurement of event shapes in deep inelastic scattering at HERA*, *Eur. Phys. J. C* **27** (2003) 531 [hep-ex/0211040] [INSPIRE].

[12] ZEUS collaboration, *Event shapes in deep inelastic scattering at HERA*, *Nucl. Phys. B* **767** (2007) 1 [hep-ex/0604032] [INSPIRE].

[13] JADE collaboration, *Measurement of the strong coupling α_S from the three-jet rate in e^+e^--annihilation using JADE data*, *Eur. Phys. J. C* **73** (2013) 2332 [arXiv:1205.3714] [INSPIRE].

[14] ALEPH et al. collaborations, *Search for charged Higgs bosons: combined results using LEP data*, *Eur. Phys. J. C* **73** (2013) 2463 [arXiv:1301.6065] [INSPIRE].

[15] DELPHI collaboration, *Measurement of the electron structure function F_2^e at LEP energies*, *Phys. Lett. B* **737** (2014) 39 [INSPIRE].

[16] OPAL collaboration, *Measurement of observables sensitive to coherence effects in hadronic Z decays with the OPAL detector at LEP*, *Eur. Phys. J. C* **75** (2015) 571 [arXiv:1505.01636] [INSPIRE].

[17] A. Badea et al., *Measurements of two-particle correlations in e^+e^- collisions at 91 GeV with ALEPH archived data*, *Phys. Rev. Lett.* **123** (2019) 212002 [arXiv:1906.00489] [INSPIRE].

[18] Y. Chen et al., *Jet energy spectrum and substructure in e^+e^- collisions at 91.2 GeV with ALEPH archived data*, *JHEP* **06** (2022) 008 [arXiv:2111.09914] [INSPIRE].

[19] A. Accardi et al., *Electron ion collider: the next QCD frontier. Understanding the glue that binds us all*, *Eur. Phys. J. A* **52** (2016) 268 [arXiv:1212.1701] [INSPIRE].

[20] R. Abdul Khalek et al., *Science requirements and detector concepts for the electron-ion collider: EIC yellow report*, *Nucl. Phys. A* **1026** (2022) 122447 [arXiv:2103.05419] [INSPIRE].

[21] LHeC Study Group collaboration, *A Large Hadron Electron collider at CERN: report on the physics and design concepts for machine and detector*, *J. Phys. G* **39** (2012) 075001 [arXiv:1206.2913] [INSPIRE].

[22] LHeC and FCC-he Study Group collaborations, *The Large Hadron-electron Collider at the HL-LHC*, *J. Phys. G* **48** (2021) 110501 [arXiv:2007.14491] [INSPIRE].

[23] D. Kang, C. Lee and I.W. Stewart, *Using 1-jettiness to measure 2 jets in DIS 3 ways*, *Phys. Rev. D* **88** (2013) 054004 [arXiv:1303.6952] [INSPIRE].

[24] V. Antonelli, M. Dasgupta and G.P. Salam, *Resummation of thrust distributions in DIS*, *JHEP* **02** (2000) 001 [hep-ph/9912488] [INSPIRE].

JHEP09(2023)194

[25] G.S. Chahal and F. Krauss, *Cluster hadronisation in Sherpa*, *SciPost Phys.* **13** (2022) 019 [arXiv:2203.11385] [INSPIRE].

[26] M. Knobbe, F. Krauss, D. Reichelt and S. Schumann, *Measuring hadronic Higgs boson branching ratios at future lepton colliders*, arXiv:2306.03682 [INSPIRE].

[27] A. Banfi, G.P. Salam and G. Zanderighi, *Principles of general final-state resummation and automated implementation*, *JHEP* **03** (2005) 073 [hep-ph/0407286] [INSPIRE].

[28] E. Gerwick, S. Höche, S. Marzani and S. Schumann, *Soft evolution of multi-jet final states*, *JHEP* **02** (2015) 106 [arXiv:1411.7325] [INSPIRE].

[29] S. Höche, S. Kuttimalai and Y. Li, *Hadronic final states in DIS at NNLO QCD with parton showers*, *Phys. Rev. D* **98** (2018) 114013 [arXiv:1809.04192] [INSPIRE].

[30] D. Reichelt et al., *Phenomenology of jet angularities at the LHC*, *JHEP* **03** (2022) 131 [arXiv:2112.09545] [INSPIRE].

[31] H1 collaboration, *Measurement of* 1*-jettiness in deep-inelastic scattering at HERA*, *PoS* **EPS-HEP2021** (2022) 367 [arXiv:2111.11364] [INSPIRE].

[32] J. Hessler, *Measurement of the* 1*-jettiness event shape observable in deep-inelastic electron-proton scattering*, Master's thesis, Tech. U., Munich, Germany (2021) [INSPIRE].

[33] H1 collaboration, *Unbinned deep learning jet substructure measurement in high* Q^2*ep collisions at HERA*, arXiv:2303.13620 [INSPIRE].

[34] T. Carli, T. Gehrmann and S. Höche, *Hadronic final states in deep-inelastic scattering with Sherpa*, *Eur. Phys. J. C* **67** (2010) 73 [arXiv:0912.3715] [INSPIRE].

[35] A.J. Larkoski, S. Marzani, G. Soyez and J. Thaler, *Soft drop*, *JHEP* **05** (2014) 146 [arXiv:1402.2657] [INSPIRE].

[36] J.M. Butterworth, A.R. Davison, M. Rubin and G.P. Salam, *Jet substructure as a new Higgs search channel at the LHC*, *Phys. Rev. Lett.* **100** (2008) 242001 [arXiv:0802.2470] [INSPIRE].

[37] M. Dasgupta, A. Fregoso, S. Marzani and G.P. Salam, *Towards an understanding of jet substructure*, *JHEP* **09** (2013) 029 [arXiv:1307.0007] [INSPIRE].

[38] J. Baron, S. Marzani and V. Theeuwes, *Soft-drop thrust*, *JHEP* **08** (2018) 105 [*Erratum ibid.* **05** (2019) 056] [arXiv:1803.04719] [INSPIRE].

[39] S. Marzani et al., *Fitting the strong coupling constant with soft-drop thrust*, *JHEP* **11** (2019) 179 [arXiv:1906.10504] [INSPIRE].

[40] J. Baron et al., *Soft-drop grooming for hadronic event shapes*, *JHEP* **07** (2021) 142 [arXiv:2012.09574] [INSPIRE].

[41] Y. Makris, *Revisiting the role of grooming in DIS*, *Phys. Rev. D* **103** (2021) 054005 [arXiv:2101.02708] [INSPIRE].

[42] M. Arratia et al., *Asymmetric jet clustering in deep-inelastic scattering*, *Phys. Rev. D* **104** (2021) 034005 [arXiv:2006.10751] [INSPIRE].

[43] *The Sherpa-*3.0.*beta code webpage*, https://sherpa-team.gitlab.io/changelog.html.

[44] SHERPA collaboration, *Event generation with Sherpa* 2.2, *SciPost Phys.* **7** (2019) 034 [arXiv:1905.09127] [INSPIRE].

JHEP09(2023)194

[45] M. Schönherr, *An automated subtraction of NLO EW infrared divergences*, *Eur. Phys. J. C* **78** (2018) 119 [arXiv:1712.07975] [INSPIRE].

[46] M. Schönherr, *Next-to-leading order electroweak corrections to off-shell WWW production at the LHC*, *JHEP* **07** (2018) 076 [arXiv:1806.00307] [INSPIRE].

[47] S. Bräuer et al., *Fixed-order and merged parton-shower predictions for WW and WWj production at the LHC including NLO QCD and EW corrections*, *JHEP* **10** (2020) 159 [arXiv:2005.12128] [INSPIRE].

[48] E. Bothmann and D. Napoletano, *Automated evaluation of electroweak Sudakov logarithms in Sherpa*, *Eur. Phys. J. C* **80** (2020) 1024 [arXiv:2006.14635] [INSPIRE].

[49] E. Bothmann et al., *Higher-order EW corrections in ZZ and ZZj production at the LHC*, *JHEP* **06** (2022) 064 [arXiv:2111.13453] [INSPIRE].

[50] *YAML: YAML Ain't Markup Language webpage*, https://yaml.org/.

[51] C. Bierlich et al., *Robust independent validation of experiment and theory: Rivet version* 3, *SciPost Phys.* **8** (2020) 026 [arXiv:1912.05451] [INSPIRE].

[52] M. Cacciari, G.P. Salam and G. Soyez, *FastJet user manual*, *Eur. Phys. J. C* **72** (2012) 1896 [arXiv:1111.6097] [INSPIRE].

[53] S. Schumann and F. Krauss, *A parton shower algorithm based on Catani-Seymour dipole factorisation*, *JHEP* **03** (2008) 038 [arXiv:0709.1027] [INSPIRE].

[54] S. Höche, F. Krauss, M. Schönherr and F. Siegert, *QCD matrix elements + parton showers: the NLO case*, *JHEP* **04** (2013) 027 [arXiv:1207.5030] [INSPIRE].

[55] S. Höche, F. Krauss, S. Schumann and F. Siegert, *QCD matrix elements and truncated showers*, *JHEP* **05** (2009) 053 [arXiv:0903.1219] [INSPIRE].

[56] F. Buccioni et al., *OpenLoops* 2, *Eur. Phys. J. C* **79** (2019) 866 [arXiv:1907.13071] [INSPIRE].

[57] A. Denner, S. Dittmaier and L. Hofer, *Collier: a fortran-based Complex One-Loop LIbrary in Extended Regularizations*, *Comput. Phys. Commun.* **212** (2017) 220 [arXiv:1604.06792] [INSPIRE].

[58] T. Gleisberg and S. Höche, *Comix, a new matrix element generator*, *JHEP* **12** (2008) 039 [arXiv:0808.3674] [INSPIRE].

[59] A. Buckley et al., *LHAPDF6: parton density access in the LHC precision era*, *Eur. Phys. J. C* **75** (2015) 132 [arXiv:1412.7420] [INSPIRE].

[60] PDF4LHC Working Group collaboration, *The PDF4LHC21 combination of global PDF fits for the LHC run III*, *J. Phys. G* **49** (2022) 080501 [arXiv:2203.05506] [INSPIRE].

[61] E. Bothmann, M. Schönherr and S. Schumann, *Reweighting QCD matrix-element and parton-shower calculations*, *Eur. Phys. J. C* **76** (2016) 590 [arXiv:1606.08753] [INSPIRE].

[62] J.-C. Winter, F. Krauss and G. Soff, *A modified cluster hadronization model*, *Eur. Phys. J. C* **36** (2004) 381 [hep-ph/0311085] [INSPIRE].

[63] T. Gleisberg et al., *Event generation with SHERPA* 1.1, *JHEP* **02** (2009) 007 [arXiv:0811.4622] [INSPIRE].

[64] G. Marchesini and B.R. Webber, *Simulation of QCD jets including soft gluon interference*, *Nucl. Phys. B* **238** (1984) 1 [INSPIRE].

JHEP09(2023)194

[65] B.R. Webber, *A QCD model for jet fragmentation including soft gluon interference*, *Nucl. Phys. B* **238** (1984) 492 [INSPIRE].

[66] D. Amati and G. Veneziano, *Preconfinement as a property of perturbative QCD*, *Phys. Lett. B* **83** (1979) 87 [INSPIRE].

[67] B. Andersson, G. Gustafson, G. Ingelman and T. Sjostrand, *Parton fragmentation and string dynamics*, *Phys. Rept.* **97** (1983) 31 [INSPIRE].

[68] M. Krishnamoorthy et al., *Apprentice for event generator tuning*, *EPJ Web Conf.* **251** (2021) 03060 [arXiv:2103.05748] [INSPIRE].

[69] H1 collaboration, *Measurements of transverse energy flow in deep inelastic scattering at HERA*, *Eur. Phys. J. C* **12** (2000) 595 [hep-ex/9907027] [INSPIRE].

[70] H1 collaboration, *Energy flow and charged particle spectrum in deep inelastic scattering at HERA*, *Z. Phys. C* **63** (1994) 377 [INSPIRE].

[71] ZEUS collaboration, *Measurement of multiplicity and momentum spectra in the current fragmentation region of the Breit frame at HERA*, *Z. Phys. C* **67** (1995) 93 [hep-ex/9501012] [INSPIRE].

[72] H1 collaboration, *Charged particle multiplicities in deep inelastic scattering at HERA*, *Z. Phys. C* **72** (1996) 573 [hep-ex/9608011] [INSPIRE].

[73] H1 collaboration, *A study of the fragmentation of quarks in e^-p collisions at HERA*, *Nucl. Phys. B* **445** (1995) 3 [hep-ex/9505003] [INSPIRE].

[74] H1 collaboration, *Evolution of ep fragmentation and multiplicity distributions in the Breit frame*, *Nucl. Phys. B* **504** (1997) 3 [hep-ex/9707005] [INSPIRE].

[75] M. Dasgupta and G.P. Salam, *Resummed event shape variables in DIS*, *JHEP* **08** (2002) 032 [hep-ph/0208073] [INSPIRE].

[76] I.W. Stewart, F.J. Tackmann and W.J. Waalewijn, *N-jettiness: an inclusive event shape to veto jets*, *Phys. Rev. Lett.* **105** (2010) 092002 [arXiv:1004.2489] [INSPIRE].

[77] T.T. Jouttenus, I.W. Stewart, F.J. Tackmann and W.J. Waalewijn, *The soft function for exclusive N-jet production at hadron colliders*, *Phys. Rev. D* **83** (2011) 114030 [arXiv:1102.4344] [INSPIRE].

[78] Z.-B. Kang, S. Mantry and J.-W. Qiu, *N-jettiness as a probe of nuclear dynamics*, *Phys. Rev. D* **86** (2012) 114011 [arXiv:1204.5469] [INSPIRE].

[79] Z.-B. Kang, X. Liu, S. Mantry and J.-W. Qiu, *Probing nuclear dynamics in jet production with a global event shape*, *Phys. Rev. D* **88** (2013) 074020 [arXiv:1303.3063] [INSPIRE].

[80] D. Kang, C. Lee and I.W. Stewart, *Analytic calculation of 1-jettiness in DIS at $\mathcal{O}(\alpha_s)$*, *JHEP* **11** (2014) 132 [arXiv:1407.6706] [INSPIRE].

[81] Z.-B. Kang, X. Liu and S. Mantry, *1-jettiness DIS event shape: NNLL+NLO results*, *Phys. Rev. D* **90** (2014) 014041 [arXiv:1312.0301] [INSPIRE].

[82] D. Kang, C. Lee and I.W. Stewart, *DIS event shape at N^3LL*, *PoS* **DIS2015** (2015) 142 [INSPIRE].

[83] C. Frye, A.J. Larkoski, M.D. Schwartz and K. Yan, *Factorization for groomed jet substructure beyond the next-to-leading logarithm*, *JHEP* **07** (2016) 064 [arXiv:1603.09338] [INSPIRE].

JHEP09(2023)194

[84] A.H. Hoang, S. Mantry, A. Pathak and I.W. Stewart, *Nonperturbative corrections to soft drop jet mass*, *JHEP* **12** (2019) 002 [arXiv:1906.11843] [INSPIRE].

[85] N. Baberuxki, C.T. Preuss, D. Reichelt and S. Schumann, *Resummed predictions for jet-resolution scales in multijet production in e^+e^- annihilation*, *JHEP* **04** (2020) 112 [arXiv:1912.09396] [INSPIRE].

[86] M. Ritzmann and W.J. Waalewijn, *Fragmentation in jets at NNLO*, *Phys. Rev. D* **90** (2014) 054029 [arXiv:1407.3272] [INSPIRE].

[87] S. Caletti et al., *Jet angularities in Z+jet production at the LHC*, *JHEP* **07** (2021) 076 [arXiv:2104.06920] [INSPIRE].

[88] S. Caletti, O. Fedkevych, S. Marzani and D. Reichelt, *Tagging the initial-state gluon*, *Eur. Phys. J. C* **81** (2021) 844 [arXiv:2108.10024] [INSPIRE].

[89] T. Gleisberg and F. Krauss, *Automating dipole subtraction for QCD NLO calculations*, *Eur. Phys. J. C* **53** (2008) 501 [arXiv:0709.2881] [INSPIRE].

[90] S. Actis et al., *RECOLA: REcursive Computation of One-Loop Amplitudes*, *Comput. Phys. Commun.* **214** (2017) 140 [arXiv:1605.01090] [INSPIRE].

[91] B. Biedermann et al., *Automation of NLO QCD and EW corrections with Sherpa and Recola*, *Eur. Phys. J. C* **77** (2017) 492 [arXiv:1704.05783] [INSPIRE].

[92] F. Cascioli, P. Maierhofer and S. Pozzorini, *Scattering amplitudes with open loops*, *Phys. Rev. Lett.* **108** (2012) 111601 [arXiv:1111.5206] [INSPIRE].

[93] M. Dobbs and J.B. Hansen, *The HepMC C++ Monte Carlo event record for high energy physics*, *Comput. Phys. Commun.* **134** (2001) 41 [INSPIRE].

[94] M. Dasgupta et al., *Parton showers beyond leading logarithmic accuracy*, *Phys. Rev. Lett.* **125** (2020) 052002 [arXiv:2002.11114] [INSPIRE].

[95] J.R. Forshaw, J. Holguin and S. Plätzer, *Building a consistent parton shower*, *JHEP* **09** (2020) 014 [arXiv:2003.06400] [INSPIRE].

[96] F. Herren et al., *A new approach to color-coherent parton evolution*, arXiv:2208.06057 [INSPIRE].

[97] M. van Beekveld and S. Ferrario Ravasio, *Next-to-leading-logarithmic PanScales showers for deep inelastic scattering and vector boson fusion*, arXiv:2305.08645 [INSPIRE].

[98] S. Höche, D. Reichelt and F. Siegert, *Momentum conservation and unitarity in parton showers and NLL resummation*, *JHEP* **01** (2018) 118 [arXiv:1711.03497] [INSPIRE].

[99] H1 collaboration, *Measurement of charged particle transverse momentum spectra in deep inelastic scattering*, *Nucl. Phys. B* **485** (1997) 3 [hep-ex/9610006] [INSPIRE].

JHEP09(2023)194